

MACHINE LEARNING-DRIVEN AERODYNAMIC SHAPE OPTIMIZATION OF NACA AIRFOILS UNDER GEOMETRIC DESIGN CONSTRAINTS

Muhammad Shaaban Abulela[1] & Mohammad Irfan Alam[1,2]

[1]Department of Aerospace Engineering, King Fahd University of Petroleum and Minerals, Dhahran, Saudi Arabia.
[2]Interdisciplinary Research Centre for Aviation and Space Exploration, King Fahd University of Petroleum and Minerals, Dhahran, Saudi Arabia.

Abstract

This study presents an automated framework for aerodynamic shape optimization of NACA four-digit airfoils using CFD-based surrogate modeling and XFOIL-based machine learning. A high-fidelity Python–ICEM–ANSYS Fluent workflow is first developed for automated geometry generation, structured meshing, CFD simulation, and aerodynamic data extraction. The CFD setup is validated using the NACA 0012 airfoil at $Re = 6 \times 10^6$, and a database of 200 NACA airfoils is generated at $\alpha = 15^\circ$. A Kriging surrogate model is then trained to predict the lift-to-drag ratio, C_l/C_d, as a function of maximum camber, camber position, and thickness. The surrogate achieves $R^2 = 0.9503$ and predicts an optimal airfoil with $C_l/C_d = 61.89$, which is verified by independent CFD with $C_l/C_d = 61.52$, corresponding to a deviation of 0.60%. The same framework is also applied to inverse design and wing-box-constrained optimization, where the best feasible constrained airfoil achieves $C_l/C_d = 60.21$. A complementary XFOIL-generated database containing $10,200$ samples is developed over $-5^\circ \leq \alpha \leq 20^\circ$ at the same Reynolds number. ANN, DNN, and LSTM/RNN models are trained using an airfoil-wise data split. The DNN provides the best predictive performance, with $RMSE = 3.282$ and $R^2 = 0.9954$ for C_l/C_d. DNN-based forward design predicts a maximum $C_l/C_d = 192.32$, and independent XFOIL re-evaluation gives $C_l/C_d = 191.93$. The results demonstrate that the proposed framework enables efficient forward optimization, inverse design, constrained optimization, and data-driven aerodynamic prediction within a unified NACA airfoil design environment.

Keywords: NACA airfoils, airfoil optimization, surrogate modeling, machine learning, XFOIL

1. Introduction

Aerodynamic shape optimization remains an important component of aircraft design because improvements in aerodynamic efficiency can directly reduce fuel consumption, operating cost, and environmental impact [1,2]. Among aerodynamic components, airfoils play a central role in determining lift generation, drag characteristics, stall behavior, and overall wing performance [3,4]. Consequently, efficient and reliable methodologies for airfoil analysis and optimization continue to receive significant attention in both academic and industrial research.

Traditional aerodynamic optimization commonly relies on high-fidelity computational fluid dynamics (CFD) coupled with gradient-based or evolutionary optimization algorithms. Although such methods can provide accurate aerodynamic predictions, they often require many expensive flow simulations, particularly when large design spaces or multiple design objectives are considered [5]. To reduce this cost, surrogate-based optimization methods have been widely adopted. Kriging and Gaussian-process-based models are especially attractive because they provide accurate response approximations using a limited number of high-fidelity samples and can be coupled efficiently with optimization algorithms [6–8]. Recent studies have further improved surrogate-assisted aerodynamic optimization through hierarchical and multi-fidelity Kriging formulations [9,10].

The choice of geometric parameterization strongly influences the efficiency and interpretability of airfoil optimization. Several approaches have been developed, including PARSEC, class-shape transformation (CST), Bézier curves, B-splines, free-form deformation, and latent-space representations [11–13]. While advanced parameterizations offer high geometric flexibility, the NACA four-digit representation remains useful for surrogate-based studies because it describes the airfoil using a small number of physically meaningful parameters: maximum camber, camber position, and maximum thickness. This simplicity facilitates design-space exploration, inverse design, and interpretation of the aerodynamic influence of each design variable.

In parallel with surrogate modeling, machine-learning techniques have increasingly been used for aerodynamic prediction and preliminary airfoil design. Recent reviews and aerodynamic analysis tools have shown the growing potential of deep-learning-based surrogate models for airfoil and blade-profile applications [14, 15]. Artificial neural networks and deep neural networks have also demonstrated strong capability for predicting aerodynamic coefficients and modeling nonlinear relationships between airfoil geometry, operating conditions, and aerodynamic performance [16, 17]. Multi-task learning frameworks have further been used to predict aerodynamic coefficients, pressure distributions, and flow-field quantities within unified data-driven models [18,19]. In addition, physics-informed learning and long short-term memory networks have been explored for aerodynamic surrogate modeling, optimization, and inverse airfoil design [20, 21].

Despite these advances, several limitations remain. Many CFD-based optimization studies are restricted by the small number of high-fidelity samples available for surrogate construction. Forward optimization, inverse design, and constrained optimization are also often treated separately rather than within a unified workflow. Furthermore, many modern machine-learning approaches rely on complex or latent geometric representations that can reduce physical interpretability. Practical geometric requirements, such as internal volume for structural members and fuel storage, are also frequently neglected during airfoil optimization, even though such constraints are important in aircraft design [22].

The present work addresses these limitations by developing an automated aerodynamic design framework for NACA four-digit airfoils that combines high-fidelity CFD-based surrogate optimization with XFOIL-based machine-learning prediction. The first component of the framework uses an integrated Python–ICEM–ANSYS Fluent workflow to automatically generate airfoil coordinates, construct structured meshes, perform CFD simulations, and extract aerodynamic coefficients. A CFD database of 200 NACA airfoils is generated at $Re = 6 \times 10^6$ and $\alpha = 15^\circ$, and a Kriging surrogate model is constructed for forward optimization, inverse design, and wing-box-constrained optimization. Independent CFD simulations are used to verify the surrogate-predicted designs.

The second component develops a complementary XFOIL-generated aerodynamic database for the same NACA design space over an angle-of-attack range from -5° to 20° at $Re = 6 \times 10^6$ [23]. The resulting dataset contains 10,200 aerodynamic samples and is used to train and compare artificial neural network (ANN), deep neural network (DNN), and long short-term memory/recurrent neural network (LSTM/RNN) models. The best-performing model is then applied to forward airfoil design, and the resulting machine-learning-generated optimum is independently re-evaluated using XFOIL.

The main contributions of this work are as follows:

1. development of a fully automated Python–ICEM–ANSYS Fluent workflow for CFD database generation of NACA four-digit airfoils;
2. construction of a CFD-based Kriging surrogate for forward optimization, inverse design, and independent CFD verification;
3. incorporation of a simplified wing-box-volume constraint to account for practical internal-volume requirements;
4. generation of a 10,200-sample XFOIL aerodynamic database over a broad angle-of-attack range;
5. comparison of ANN, DNN, and LSTM/RNN models for aerodynamic prediction and application of the best-performing model to forward design.

The remainder of this paper is organized as follows. The next section presents the CFD validation study, including the numerical setup, mesh independence analysis, and comparison with experimental data for the NACA 0012 airfoil. The methodology section then describes the NACA parameterization, database generation procedures, Kriging surrogate formulation, optimization problems, XFOIL database, and machine-learning models. The results section presents the CFD–Kriging optimization results, inverse-design verification, constrained optimization results, XFOIL–ML model comparison, DNN-based forward design, and sensitivity analysis. Finally, the conclusions summarize the main findings, limitations, and future work.

2. CFD Validation

Before generating the aerodynamic database used for surrogate-model construction, the numerical CFD setup was validated using the NACA 0012 airfoil at $Re = 6 \times 10^6$. This validation case was selected because the NACA 0012 airfoil is a standard benchmark for two-dimensional airfoil simulations and because experimental aerodynamic data are available from Ladson [24]. ICEM CFD 2024 R2 was used for mesh generation, while ANSYS Fluent 2024 R2 was employed to solve the two-dimensional, steady, incompressible Reynolds-Averaged Navier–Stokes equations using the SST k–ω turbulence model.

The computational domain employed a structured C-type topology. The upstream boundary was located $20c$ ahead of the airfoil leading edge, the downstream boundary extended $35c$ behind the trailing edge, and the upper and lower far-field boundaries were positioned $20c$ from the chord line. A velocity-inlet boundary condition was specified to achieve the target Reynolds number, while the outlet was defined as a pressure outlet. The airfoil surface was modeled as a stationary no-slip wall. A pressure-based coupled solver was used with second-order upwind discretization. Residual convergence criteria were set to 10^{-6} for continuity and momentum and 10^{-5} for turbulence quantities. The first-layer mesh spacing was selected to achieve $y^+ \approx 1$. The main numerical settings are summarized in Table 1.

Table 1 – Simulation parameters used in the numerical study.

Parameter	Value
Solver	Pressure-based, steady-state, coupled
Viscous model	SST k–ω
Inlet velocity, V_∞	87.6441 m/s ($Re = 6 \times 10^6$)
Density, ρ	1.225 kg/m^3
Viscosity, μ	1.7894×10^{-5} Pa·s
Chord length, c	1 m (Normalized)
Momentum discretization	Second-order upwind
Residual criteria	10^{-6} continuity/momentum; 10^{-5} turbulence
Near-wall resolution	$y^+ \approx 1$
Domain dimensions	$20c$ upstream, $35c$ downstream, $20c$ far field

2.1 Mesh Independence Analysis

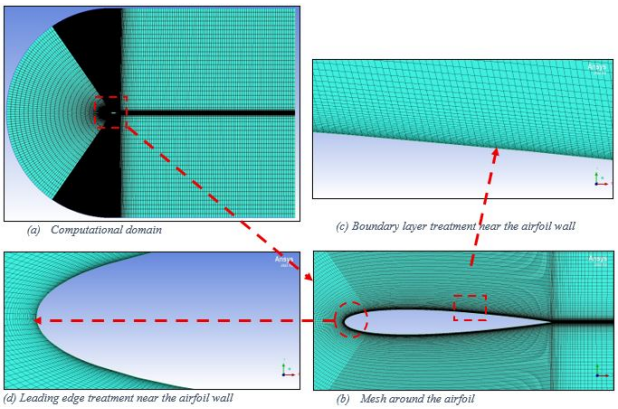
A mesh independence study was conducted at $\alpha = 15^\circ$ to ensure that the predicted aerodynamic coefficients were not significantly affected by grid resolution. This operating condition corresponds to a high-lift case near the stall region and therefore provides a demanding condition for assessing grid sensitivity.

Five structured C-type meshes were tested, with cell counts ranging from 17,018 to 143,379. For each grid, the lift coefficient (C_l), drag coefficient (C_d), and lift-to-drag ratio (C_l/C_d) were evaluated. As shown in Table 2, the aerodynamic coefficients converge progressively with mesh refinement. The differences between Grid 4 and Grid 5 are only 0.05% for C_l, 0.16% for C_d, and 0.21% for C_l/C_d. Therefore, Grid 4, consisting of 75,027 cells, was selected for all subsequent CFD simulations because it provides a suitable balance between numerical accuracy and computational cost.

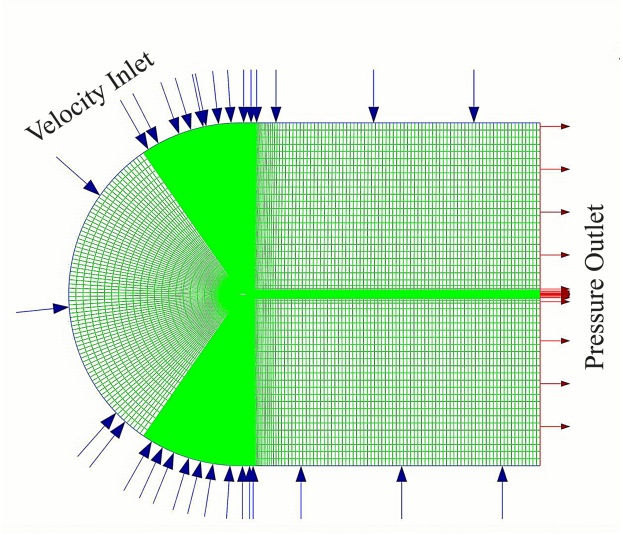
Table 2 – Mesh independence analysis at $\alpha = 15^\circ$.

Grid	No. Cells	C_l	C_d	C_l/C_d	C_l Error (%)	C_d Error (%)	C_l/C_d Error (%)
1	17,018	1.4514	0.02725	53.25763	–	–	–
2	30,121	1.4544	0.02708	53.7103	0.20	0.64	0.85
3	53,417	1.4578	0.02694	54.1065	0.23	0.50	0.74
4	75,027	1.4606	0.02689	54.3268	0.19	0.21	0.41
5	143,379	1.4613	0.02684	54.4430	0.05	0.16	0.21

The structured C-type mesh topology and boundary-condition setup are shown in Fig. 1. The mesh provides near-wall refinement around the airfoil and sufficient far-field spacing to reduce boundary effects.



(a) Structured C-type computational domain.



(b) Imported mesh and boundary-condition setup in ANSYS Fluent.

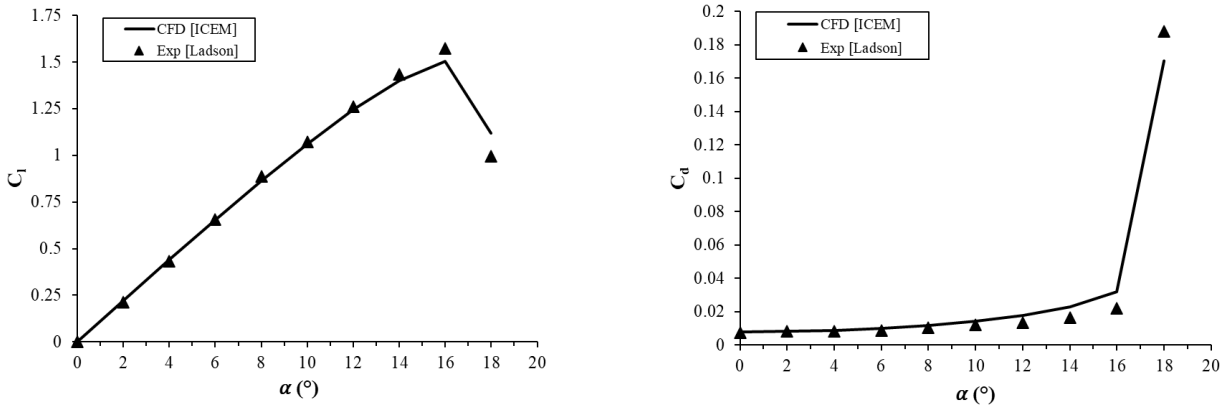
Figure 1 – Structured C-type computational domain and boundary-condition setup used for the CFD simulations.

2.2 Experimental Validation: NACA 0012

The selected mesh and solver configuration were validated against experimental measurements for the NACA 0012 airfoil at $Re = 6 \times 10^6$ reported by Ladson [24]. Figure 2 compares the predicted lift and drag coefficients with the experimental data over the investigated angle-of-attack range.

Good agreement is observed across the linear lift region and near the stall onset. The SST k–ω model captures the lift-curve slope and the overall stall behavior with satisfactory accuracy, while the drag coefficient trend is also reproduced well across the investigated range. These results indicate that the selected numerical setup provides reliable prediction of the integral aerodynamic coefficients required for database generation.

Further validation was performed using the pressure coefficient distribution at $\alpha = 15^\circ$, as shown in Fig. 3. The numerical results show good agreement with the experimental data over most of the chord on both the pressure and suction surfaces. A localized discrepancy is observed near the leading edge, where the fully turbulent SST k–ω simulation overpredicts the suction peak. This discrepancy is consistent with the known sensitivity of near-stall leading-edge pressure predictions to transition and localized separation effects. Despite this local difference, the downstream pressure recovery and the integrated aerodynamic coefficients are captured with sufficient accuracy for the objectives of the present study. Therefore, the validated CFD configuration is adopted for the automated generation of the aerodynamic database used in the surrogate-based optimization framework.



(a) C_l vs. angle of attack.

(b) C_d vs. angle of attack.

Figure 2 – Validation of CFD predictions against experimental data for NACA 0012 at $Re = 6 \times 10^6$.

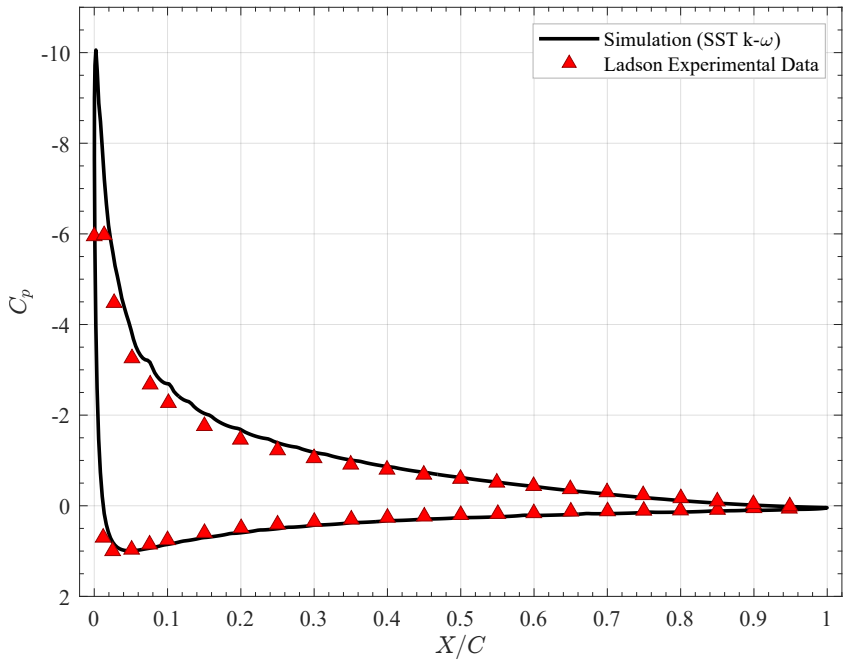


Figure 3 – Pressure coefficient distribution for NACA 0012 at $\alpha = 15^\circ$ and $Re = 6 \times 10^6$.

3. Methodology

The proposed methodology consists of two complementary frameworks. The first framework uses high-fidelity CFD simulations and Kriging surrogate modeling for forward optimization, inverse airfoil design, and wing-box-constrained optimization of NACA four-digit airfoils. The second framework uses a larger XFOIL-generated aerodynamic database to train and compare machine-learning models for aerodynamic prediction and forward design. The CFD–Kriging framework provides high-fidelity verification at a selected operating condition, while the XFOIL–ML framework extends the analysis over a broader angle-of-attack range. The following subsections describe the common NACA parameterization, database-generation procedures, surrogate formulation, optimization problems, and machine-learning models.

3.1 Overall Framework

The CFD-based framework integrates airfoil geometry generation, structured meshing, CFD simulation, aerodynamic data extraction, surrogate training, optimization, and independent CFD verification within a unified Python–ICEM–ANSYS Fluent workflow. NACA four-digit airfoils are parameterized using three design variables: maximum camber (m), camber position (p), and maximum thickness (t). For each candidate geometry, structured C-type meshes are generated in ICEM CFD, and steady incompressible RANS simulations are performed in ANSYS Fluent using the validated SST k–ω setup. The resulting C_l, C_d, and C_l/C_d values are stored in a CFD database and used to train the Kriging surrogate. The trained surrogate is then used for forward optimization, inverse design, and wing-box-constrained optimization, while selected candidates are verified using independent CFD simulations. The complete CFD–Kriging workflow is summarized in Fig. 4.

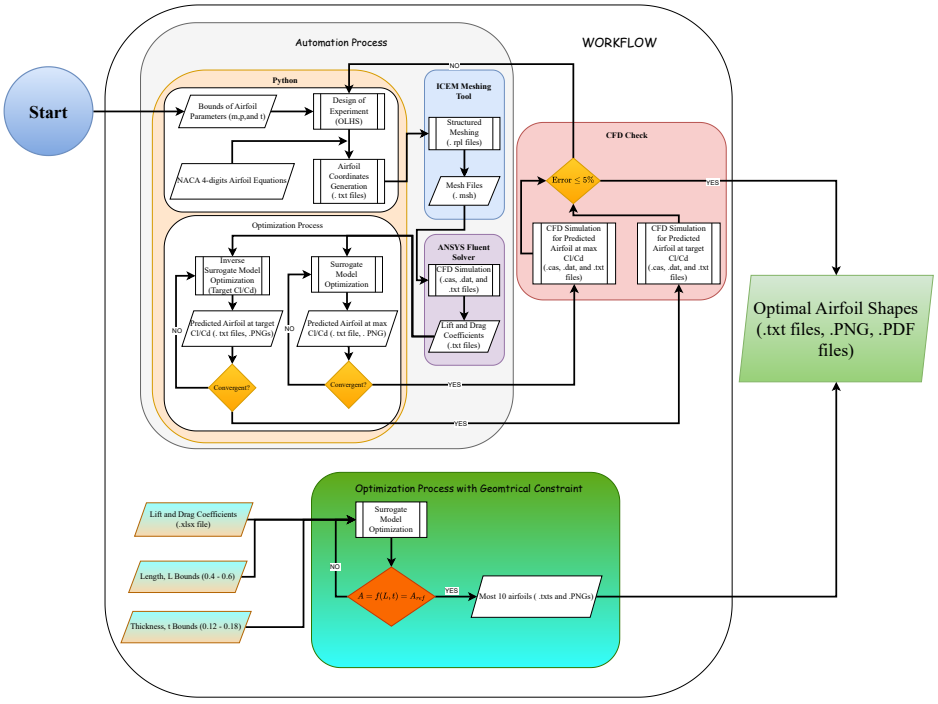


Figure 4 – Fully automated Python–ICEM–ANSYS Fluent surrogate-assisted airfoil optimization framework.

To complement the fixed-condition CFD database, the second framework uses XFOIL to generate a larger aerodynamic database over a wider operating envelope. The same 200 NACA airfoil geometries are evaluated over an angle-of-attack range of $-5^\circ \leq \alpha \leq 20^\circ$ with increments of 0.5° at $Re = 6 \times 10^6$. Since each airfoil is evaluated at 51 angles of attack, the resulting dataset contains 10,200 aerodynamic samples. ANN, DNN, and LSTM/RNN models are trained and compared using this database. The best-performing model is then used for forward maximum-C_l/C_d design, and the predicted optimum is independently re-evaluated using XFOIL. The overall XFOIL–ML workflow is

shown in Fig. 5.

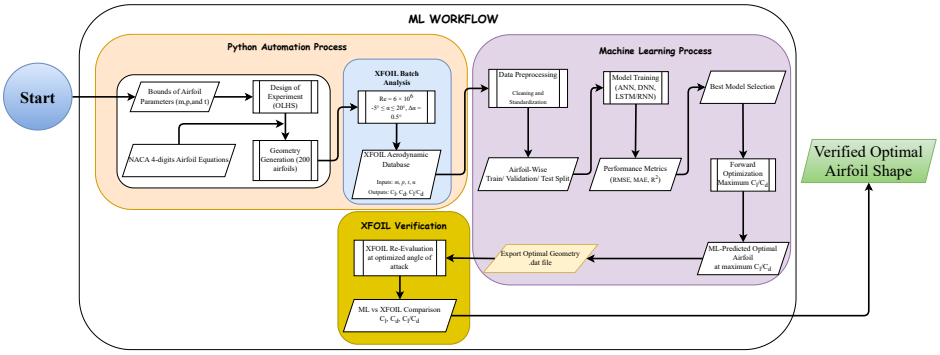


Figure 5 – XFOIL-generated database and machine-learning framework employed for aerodynamic prediction, forward design, and XFOIL-based verification.

Having introduced the two automated workflows, the following subsection defines the common NACA four-digit parameterization used to generate the airfoil geometries in both the CFD–Kriging and XFOIL–ML frameworks.

3.2 NACA Airfoil Parametrization

The airfoils considered in this study belong to the NACA four-digit series. In the NACA MPXX notation, M represents the maximum camber as a percentage of the chord, P denotes the chordwise location of maximum camber in tenths of the chord, and XX specifies the maximum thickness as a percentage of the chord. The corresponding normalized design variables are therefore $m = M/100$, $p = P/10$, and $t = XX/100$.

For a normalized chord length $c = 1$, the mean camber line is given by

$$y_c(x) = \begin{cases} \dfrac{m}{p^2}(2px - x^2), & 0 \le x < p, \\ \dfrac{m}{(1-p)^2}(1 - 2p + 2px - x^2), & p \le x \le 1. \end{cases} \tag{1}$$

$$\frac{dy_c}{dx} = \begin{cases} \dfrac{2m}{p^2}(p - x), & 0 \le x < p, \\ \dfrac{2m}{(1-p)^2}(p - x), & p \le x \le 1. \end{cases} \tag{2}$$

The thickness distribution is

$$y_t = \frac{t}{0.2}\left(a_0\sqrt{x} + a_1 x + a_2 x^2 + a_3 x^3 + a_4 x^4\right), \tag{3}$$

where $a_0 = 0.2969$, $a_1 = -0.1260$, $a_2 = -0.3516$, $a_3 = 0.2843$, and $a_4 = -0.1036$. The coefficient $a_4 = -0.1036$ is used to impose a closed trailing edge. The local surface angle is defined as $\theta = \tan^{-1}(dy_c/dx)$, and the upper and lower surface coordinates are computed as

$$x_u = x - y_t \sin\theta, \qquad y_u = y_c + y_t \cos\theta, \tag{4}$$

$$x_l = x + y_t \sin\theta, \qquad y_l = y_c - y_t \cos\theta. \tag{5}$$

Cosine spacing is applied along the chord to improve leading-edge resolution [25]:

$$x = \frac{1}{2}(1 - \cos\beta), \qquad 0 \le \beta \le \pi. \tag{6}$$

The same parameterization is used in both frameworks, with the design bounds

$$m \in [0, 0.05], \qquad p \in [0, 0.70], \qquad t \in [0.10, 0.24]. \tag{7}$$

The next step is to sample this three-dimensional NACA design space in a manner that provides adequate coverage for surrogate construction while keeping the number of high-fidelity CFD simulations manageable.

3.3 Design of Experiments

The aerodynamic design space was sampled using Optimal Latin Hypercube Sampling (OLHS) [26]. OLHS was selected because it provides a space-filling distribution of design points while reducing correlation among the design variables, which supports surrogate-model construction using a limited number of CFD simulations. A total of 200 NACA four-digit airfoil configurations were generated within the prescribed bounds of m, p, and t. These 200 geometries form the basis of the CFD database and are also used in the XFOIL–ML framework, where each airfoil is evaluated over multiple angles of attack to generate a larger machine-learning dataset.

After defining the sampled airfoil geometries, the CFD automation procedure was used to evaluate the aerodynamic performance of each design at the selected high-lift operating condition.

3.4 Automated CFD Database Generation

For each OLHS-generated airfoil, a Python-based automation workflow generated the airfoil coordinates, executed ICEM CFD replay scripts, created the structured C-type mesh, launched the ANSYS Fluent simulation, and extracted the aerodynamic coefficients. All CFD simulations were performed using the validated setup at $Re = 6 \times 10^6$ and $\alpha = 15^\circ$. This angle of attack was selected because it corresponds to a high-lift operating condition near the stall region, where aerodynamic performance is sensitive to airfoil geometry. Therefore, the resulting optimum should be interpreted as specific to this selected design condition.

The lift and drag coefficients were extracted automatically from the Fluent solution files, and the objective function was defined as

$$J(\mathbf{x}) = \frac{C_l}{C_d}, \tag{8}$$

where $\mathbf{x} = [m, p, t]^\mathsf{T}$ is the airfoil design vector. The resulting CFD database consists of 200 aerodynamic samples and is used for Kriging surrogate construction, forward optimization, inverse design, and constrained optimization. The formulation of the Kriging surrogate model used for these tasks is presented next.

3.5 Kriging Surrogate Model Formulation

Kriging, also known as Gaussian process regression, was used to approximate the CFD-computed aerodynamic response within the sampled NACA design space. This approach is suitable because high-fidelity CFD simulations are computationally expensive, while optimization requires repeated evaluations of the objective function.

Let $\mathbf{x} = [m, p, t]^\mathsf{T}$ denote the airfoil design vector and let $y(\mathbf{x}) = C_l/C_d$ represent the aerodynamic response. Given N CFD samples $\{(\mathbf{x}_i, y_i)\}_{i=1}^N$, ordinary Kriging models the response as

$$y(\mathbf{x}) = \mu + z(\mathbf{x}), \tag{9}$$

where μ is a constant trend and $z(\mathbf{x})$ is a zero-mean Gaussian process. The covariance between two sample locations is defined as

$$\mathrm{Cov}[z(\mathbf{x}_i), z(\mathbf{x}_j)] = \sigma^2 R(\mathbf{x}_i, \mathbf{x}_j), \tag{10}$$

where σ^2 is the process variance and $R(\mathbf{x}_i, \mathbf{x}_j)$ is the spatial correlation function. A squared-exponential correlation function was adopted:

$$R(\mathbf{x}_i, \mathbf{x}_j) = \exp\left[-\sum_{k=1}^{3} \theta_k (x_{i,k} - x_{j,k})^2\right], \tag{11}$$

where θ_k are positive correlation hyperparameters.

For numerical stability, a small nugget regularization was applied to the correlation matrix, $\mathbf{R}_\lambda = \mathbf{R} + \lambda \mathbf{I}$. The Kriging predictor is then expressed as

$$\hat{y}(\mathbf{x}) = \hat{\mu} + \mathbf{r}(\mathbf{x})^\mathsf{T} \mathbf{R}_\lambda^{-1} (\mathbf{y} - \mathbf{1}\hat{\mu}), \tag{12}$$

where $\hat{\mu}$ is the estimated trend, $\mathbf{y}$ is the vector of CFD responses, $\mathbf{r}(\mathbf{x})$ is the correlation vector between the prediction point and the training samples, and $\mathbf{1}$ is a vector of ones. After training, the surrogate provides a rapid approximation of the CFD response and is used for forward optimization, inverse design, and constrained optimization.

3.6 Kriging-Based Optimization Problems

The forward optimization problem seeks the airfoil geometry that maximizes the surrogate-predicted lift-to-drag ratio at the selected CFD design condition. It is formulated as

$$\max_{\mathbf{x}} \ \hat{y}(\mathbf{x}) = \max_{\mathbf{x}} \left(\frac{C_l}{C_d} \right)_{\text{surrogate}}, \tag{13}$$

subject to

$$m \in [0, 0.05], \qquad p \in [0, 0.70], \qquad t \in [0.10, 0.24]. \tag{14}$$

After the optimal geometry is identified, an independent CFD simulation is performed to verify the surrogate-predicted performance.

The same surrogate is also used for inverse design. For a prescribed target value $(C_l/C_d)_{\text{target}}$, the inverse problem is written as

$$\min_{\mathbf{x}} \left| \hat{y}(\mathbf{x}) - \left(\frac{C_l}{C_d} \right)_{\text{target}} \right|. \tag{15}$$

In this study, three target values are considered:

$$\frac{C_l}{C_d} = 30,\ 40,\ 50. \tag{16}$$

The resulting inverse-designed airfoils are also re-evaluated using independent CFD simulations.

To account for simplified internal-volume requirements, a wing-box geometric constraint is incorporated into the CFD-based optimization framework. The normalized wing-box cross-sectional area per unit span is approximated as

$$A_{wb} = tL, \tag{17}$$

where t is the airfoil thickness ratio and L is the normalized chordwise length of the assumed wing-box region. The constrained optimization is formulated as

$$\max_{m,p,t,L} \quad \hat{y}(\mathbf{x}) = \left(\frac{C_l}{C_d} \right)_{\text{surrogate}} \tag{18}$$

$$\text{s.t.} \quad A_{wb} = A_0, \tag{19}$$

$$m \in [0, 0.05], \tag{20}$$

$$p \in [0, 0.70], \tag{21}$$

$$t \in [0.12, 0.18], \tag{22}$$

$$L \in [0.40, 0.60], \tag{23}$$

where $A_0 = 0.08$ is the target normalized wing-box area. During the optimization search, candidate airfoils are considered feasible when

$$\left| \frac{A_{wb} - A_0}{A_0} \right| \leq 0.01. \tag{24}$$

This formulation allows the CFD–Kriging framework to support forward optimization, inverse design, and constrained aerodynamic optimization. Having defined the CFD-based surrogate optimization procedure, the following subsection introduces the complementary XFOIL database used for machine-learning model development.

3.7 XFOIL Database Generation

While the CFD database provides high-fidelity aerodynamic data for surrogate-assisted optimization, its size is limited by the cost of CFD simulation. Therefore, a complementary aerodynamic database was generated using XFOIL [23] to support machine-learning model development over a wider operating range. This database is not intended to replace the CFD-based framework; rather, it provides a larger dataset for evaluating data-driven aerodynamic prediction and preliminary forward design.

The same 200 NACA four-digit airfoils used in the CFD framework were analyzed using XFOIL at a fixed Reynolds number of $Re = 6 \times 10^6$. For each airfoil, aerodynamic coefficients were computed over the angle-of-attack range

$$-5^\circ \leq \alpha \leq 20^\circ, \tag{25}$$

with an increment of

$$\Delta\alpha = 0.5^\circ. \tag{26}$$

Thus, each airfoil contributes 51 operating points, resulting in

$$N = 200 \times 51 = 10,200 \tag{27}$$

aerodynamic samples.
For each sample, the machine-learning input vector is defined as

$$\mathbf{x}_{ML} = [m, p, t, \alpha]^\mathsf{T}, \tag{28}$$

where m, p, and t define the NACA geometry and α is the angle of attack. The corresponding output vector is

$$\mathbf{y}_{ML} = [C_l, C_d, C_l/C_d]^\mathsf{T}. \tag{29}$$

The Reynolds number is kept fixed for all XFOIL evaluations and is therefore not included as an independent machine-learning input. The resulting database captures aerodynamic variations due to both airfoil geometry and angle of attack and provides the basis for training the ANN, DNN, and LSTM/RNN models.
Having generated the XFOIL aerodynamic database, the next step is to preprocess the data and define a train–validation–test strategy that avoids information leakage between airfoil geometries.

3.8 Data Preprocessing and Airfoil-Wise Dataset Splitting

Prior to machine-learning model development, the XFOIL-generated database was inspected to remove missing, non-physical, or non-converged samples. The remaining valid data were arranged into a supervised learning dataset using the input vector $\mathbf{x}_{ML} = [m, p, t, \alpha]^\mathsf{T}$ and output vector $\mathbf{y}_{ML} = [C_l, C_d, C_l/C_d]^\mathsf{T}$.
To improve numerical stability during neural-network training, min–max normalization was applied to the input and output variables:

$$x_{\text{norm}} = \frac{x - x_{\min}}{x_{\max} - x_{\min}}. \tag{30}$$

This transformation maps each variable into the interval $[0, 1]$ while preserving the relative variation within the dataset.
To avoid data leakage, the dataset was divided on an airfoil-wise basis rather than by randomly splitting individual aerodynamic samples. Therefore, all angle-of-attack data associated with a given airfoil were assigned to only one subset. The 200 airfoils were divided into 128 training airfoils, 32 validation airfoils, and 40 testing airfoils. Since each airfoil was evaluated at 51 angles of attack, the corresponding sample counts are

$$N_{\text{train}} = 128 \times 51 = 6528, \tag{31}$$

$$N_{\text{val}} = 32 \times 51 = 1632, \tag{32}$$

and

$$N_{\text{test}} = 40 \times 51 = 2040. \tag{33}$$

This partitioning provides a more rigorous assessment of model generalization because the trained models are evaluated on airfoil geometries not seen during training or validation.
The preprocessed airfoil-wise dataset is then used to train and compare three machine-learning architectures, described next.

3.9 Machine-Learning Model Architectures

Three machine-learning architectures were developed and compared using the preprocessed XFOIL database: an Artificial Neural Network (ANN), a Deep Neural Network (DNN), and a Long Short-Term Memory/Recurrent Neural Network (LSTM/RNN). All models use the same aerodynamic inputs and outputs, allowing a consistent comparison of predictive accuracy and generalization capability.

The ANN is used as a baseline feedforward neural-network model for nonlinear regression. It maps the input vector $[m, p, t, \alpha]^{\mathsf{T}}$ directly to the aerodynamic outputs $[C_l, C_d, C_l/C_d]^{\mathsf{T}}$ through fully connected hidden layers. Rectified Linear Unit (ReLU) activation functions are used in the hidden layers, and the model is trained using the Adam optimizer with Mean Squared Error (MSE) as the loss function.

The DNN uses a deeper feedforward architecture than the baseline ANN. Its additional hidden layers provide greater representational capacity for learning nonlinear relationships between airfoil geometry, angle of attack, and aerodynamic performance. The DNN is also trained using ReLU activation functions, the Adam optimizer, and MSE loss. Because the XFOIL database contains 10,200 samples, it provides sufficient data for training this deeper architecture.

The LSTM/RNN model is included to examine whether explicitly learning the ordered aerodynamic response across the angle-of-attack sweep improves prediction accuracy. For each airfoil, the input sequence is represented as

$$\mathbf{X} = [\mathbf{x}_1, \mathbf{x}_2, \ldots, \mathbf{x}_T], \tag{34}$$

where

$$\mathbf{x}_t = [m, p, t, \alpha_t]^{\mathsf{T}}, \tag{35}$$

and $T = 51$ is the number of angle-of-attack points. The corresponding output at each sequence step is

$$\mathbf{y}_t = [C_l, C_d, C_l/C_d]^{\mathsf{T}}. \tag{36}$$

The LSTM/RNN model is trained using the Adam optimizer and MSE loss. This architecture is compared with the feedforward ANN and DNN models to determine whether sequence modeling provides an advantage for the present aerodynamic dataset.

After training, all models are evaluated using the same independent airfoil-wise test dataset. The performance metrics used for this comparison are defined in the following subsection.

3.10 Evaluation Metrics

The ANN, DNN, and LSTM/RNN models were evaluated on the independent airfoil-wise test set using Root Mean Squared Error (RMSE), Mean Absolute Error (MAE), and the coefficient of determination (R^2). These metrics quantify the prediction-error magnitude and goodness of fit between the model predictions and the XFOIL-generated reference data.

$$\mathrm{RMSE} = \sqrt{\frac{1}{N}\sum_{i=1}^{N}(y_i - \hat{y}_i)^2}, \quad \mathrm{MAE} = \frac{1}{N}\sum_{i=1}^{N}|y_i - \hat{y}_i|, \quad R^2 = 1 - \frac{\sum_{i=1}^{N}(y_i - \hat{y}_i)^2}{\sum_{i=1}^{N}(y_i - \bar{y})^2}. \tag{37}$$

Here, y_i and $\hat{y}_i$ are the reference and predicted values, $\bar{y}$ is the mean of the reference data, and N is the number of test samples. Lower RMSE and MAE values indicate smaller prediction errors, while R^2 values closer to unity indicate stronger agreement with the reference data.

4. Results and Discussion

This section presents the results obtained from the two complementary frameworks developed in this study. The first part discusses the CFD–Kriging framework, including CFD database generation, surrogate-model accuracy, forward optimization, inverse design, and wing-box-constrained optimization. The second part presents the XFOIL–ML framework, including model comparison, DNN-based forward design, sensitivity analysis, and comparison with the CFD-based framework.

4.1 CFD Database and Kriging Training Strategy

A total of 200 NACA four-digit airfoil configurations were generated using OLHS within the prescribed design space defined by maximum camber (m), camber position (p), and thickness ratio (t). Each airfoil was evaluated using the validated CFD setup at $\alpha = 15^\circ$ and $Re = 6 \times 10^6$. The resulting CFD database defines the nonlinear mapping

$$\mathbf{x} = [m, p, t]^\mathsf{T} \longrightarrow J(\mathbf{x}) = \frac{C_l}{C_d}. \tag{38}$$

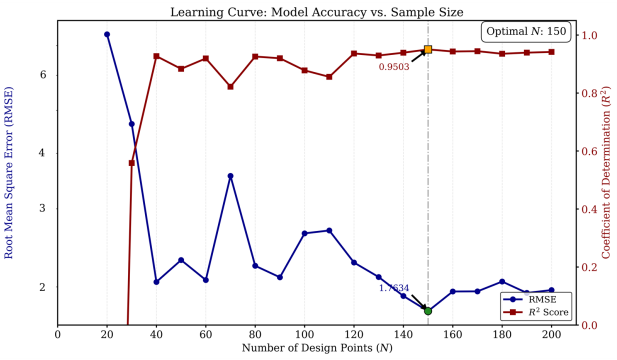
For surrogate assessment, 80% of the CFD samples were initially used for training and 20% were reserved for testing. After confirming the surrogate accuracy and convergence behavior, the final Kriging model used for optimization was retrained using the complete set of 200 CFD samples.

4.2 Kriging Surrogate Accuracy and Convergence

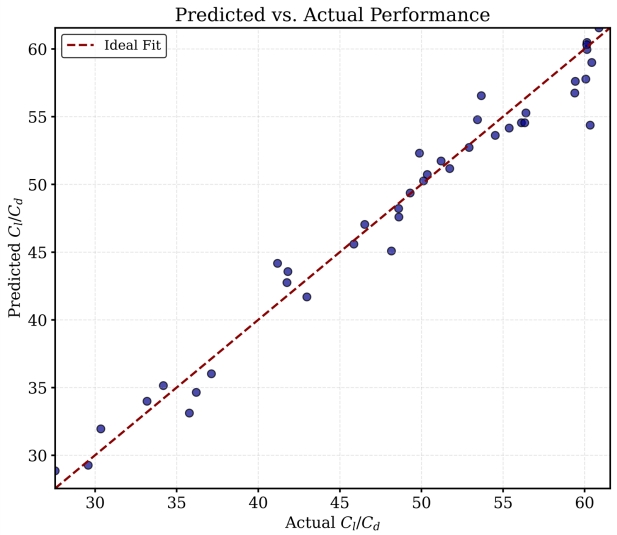
The Kriging surrogate was evaluated before applying it to the optimization studies to ensure that it could reliably approximate the CFD-computed lift-to-drag ratio within the sampled NACA design space. Figure 6 summarizes both the convergence behavior and the prediction accuracy of the trained surrogate.

As shown in Fig. 6(a), the learning curve shows the variation of RMSE and R^2 as the number of CFD training samples increases. The RMSE generally decreases as additional CFD samples are included, while the coefficient of determination approaches a stable high value. Beyond approximately 150 samples, further improvement becomes relatively small, indicating that the surrogate response has reached a stable level of accuracy within the sampled design space. The final trained model achieved $R^2 = 0.9503$, demonstrating strong predictive capability for C_l/C_d.

The predictive accuracy is further assessed in Fig. 6(b), which compares Kriging predictions with CFD results for the withheld test dataset. The predicted values follow the ideal one-to-one trend closely, confirming that the surrogate is sufficiently accurate for guiding the optimization search. Nevertheless, the final optimized candidates are independently verified using CFD.



(a) Learning curve.



(b) Predicted versus CFD.

Figure 6 – Kriging surrogate validation: (a) learning curve showing RMSE and R^2 as functions of CFD training sample size and (b) comparison between Kriging predictions and CFD results for the withheld test dataset.

After confirming the surrogate accuracy and convergence behavior, the trained Kriging model was used for forward aerodynamic optimization, as discussed next.

4.3 Kriging-Based Forward Optimization Results

After confirming the accuracy of the Kriging surrogate, the trained model was used for forward aerodynamic optimization. The objective was to maximize C_l/C_d within the prescribed NACA four-digit design-variable bounds.

Figure 7 shows the convergence history of the surrogate-based forward optimization near the optimum. The objective value stabilizes at a maximum predicted lift-to-drag ratio of

$$(C_l/C_d)_{\max}^{\text{surrogate}} = 61.89. \tag{39}$$

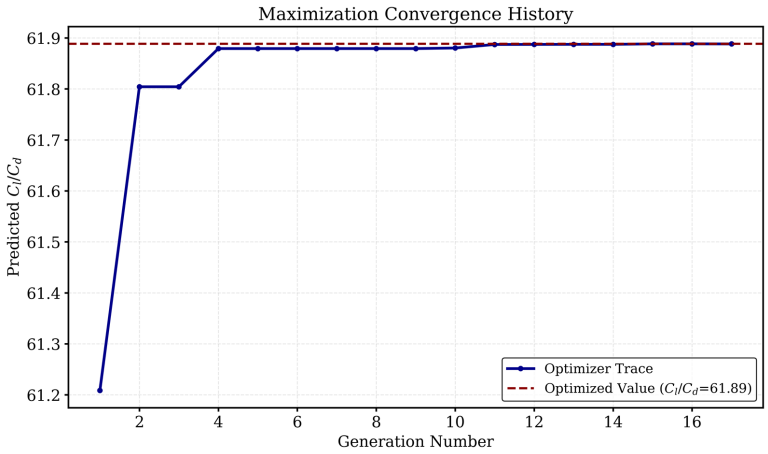


Figure 7 – Convergence history of the surrogate-based forward optimization near the maximum C_l/C_d solution.

The corresponding optimal design variables and independent CFD verification are summarized in Table 3. The optimized airfoil is characterized by moderate camber, a forward camber position, and a thickness ratio of approximately 13%, resulting in a geometry close to a NACA 2213-type airfoil.

Table 3 – Comparison between surrogate prediction and CFD results for the maximum-C_l/C_d airfoil.

m	p	t	C_l/C_d (surrogate)	C_l/C_d (CFD)	Error (%)	Approximate NACA
0.0219	0.2007	0.1298	61.89	61.52	0.60	2213

The close agreement between the surrogate prediction and the independent CFD result confirms that the Kriging surrogate can guide the forward optimization process reliably while reducing the need for repeated CFD evaluations.

The geometry of the optimized airfoil is shown in Fig. 8. The resulting shape reflects the design selected by the surrogate model to maximize aerodynamic efficiency at the fixed design condition of $\alpha = 15^\circ$ and $Re = 6 \times 10^6$.

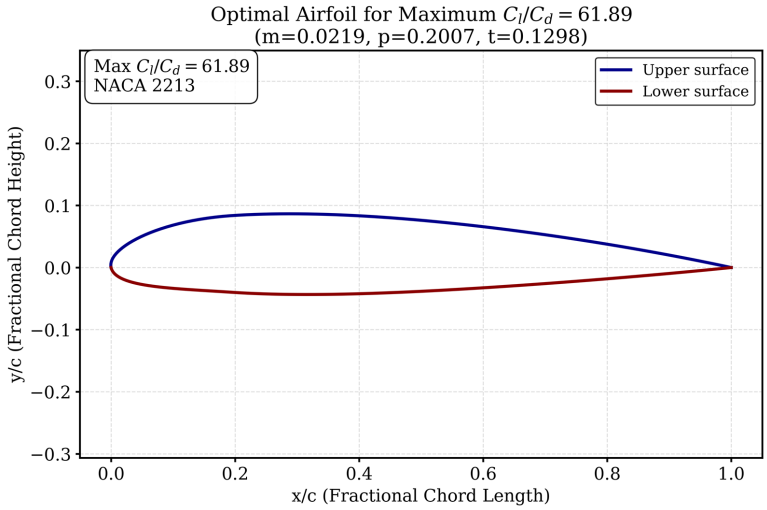


Figure 8 – Airfoil geometry predicted by the surrogate model for the maximum C_l/C_d design.

Having verified the forward optimum, the same Kriging surrogate was next used for inverse design to recover geometries corresponding to prescribed aerodynamic-efficiency targets.

4.4 Kriging-Based Inverse Design Results

The inverse-design capability of the Kriging framework was assessed using target lift-to-drag ratios of $C_l/C_d = 30$, 40, and 50. The inverse-designed airfoils and their independent CFD verification results are summarized in Table 4. The recovered geometries show systematic changes in camber, camber position, and thickness as the prescribed aerodynamic-efficiency target is varied.

Table 4 – Comparison between Kriging inverse-design targets and independent CFD verification results.

m	p	t	Target C_l/C_d (surrogate)	C_l/C_d (CFD)	Error (%)	Approximate NACA
0.0422	0.3866	0.2356	30.0	30.802	2.60	4424
0.0271	0.1999	0.2186	40.0	40.240	0.60	3222
0.0135	0.3466	0.2012	50.0	50.168	0.33	1320

The maximum deviation among the investigated targets is 2.60%, while the remaining cases show deviations below 1%. These results confirm that the Kriging surrogate can recover airfoil geometries corresponding to prescribed aerodynamic-performance targets with good accuracy.
For direct geometric comparison, all inverse-designed airfoils are superimposed in Fig. 9. The figure shows the geometric variation required to achieve different target values of C_l/C_d within the prescribed NACA design space.

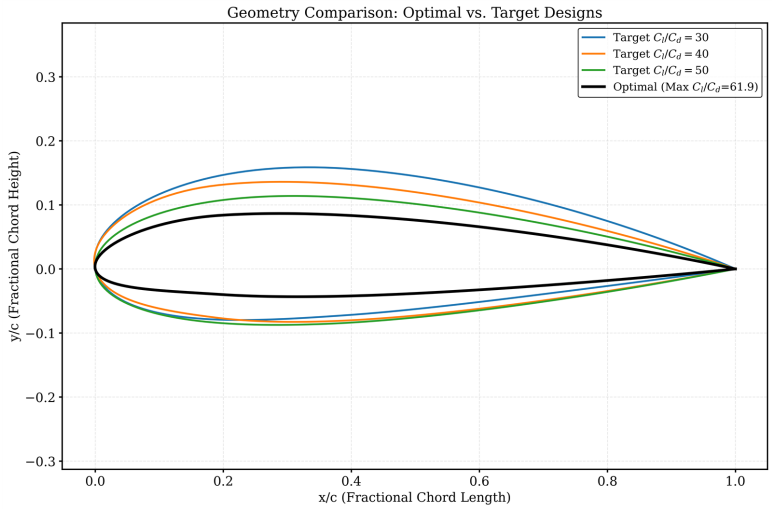


Figure 9 – Comparison of Kriging-predicted airfoil geometries for different target values of C_l/C_d.

Overall, the close agreement between the inverse-design targets and independent CFD evaluations confirms the robustness of the Kriging surrogate for both forward and inverse airfoil-design tasks. The following subsection extends this assessment by introducing a wing-box geometric constraint to examine aerodynamic performance under simplified internal-volume requirements.

4.5 Wing-Box-Constrained Kriging Optimization Results

To examine aerodynamic performance under a simplified internal-volume requirement, the wing-box geometric constraint defined in the methodology was incorporated into the CFD-based Kriging optimization process. The constraint approximates the normalized wing-box cross-sectional area per unit span as $A_{wb} = tL$, with a target value of $A_0 = 0.08$ and a 1% feasibility tolerance.

The optimal feasible design obtained under this constraint is shown in Fig. 10. The shaded region represents the assumed wing-box area between the front and rear spars. The constrained optimum achieved

$$(C_l/C_d)_{\text{constrained}} = 60.21. \tag{40}$$

Compared with the unconstrained Kriging optimum of $C_l/C_d = 61.89$, the reduction in aerodynamic efficiency is

$$\frac{61.89 - 60.21}{61.89} \times 100 = 2.71\%. \tag{41}$$

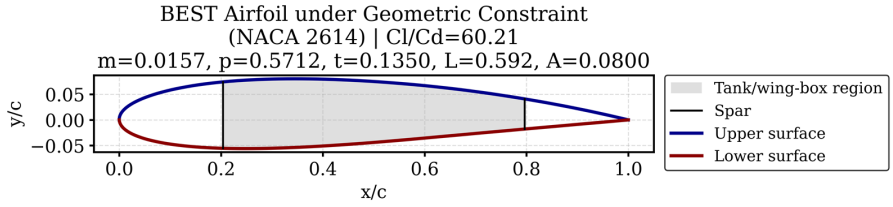


Figure 10 – Optimal airfoil obtained under the wing-box geometric constraint $(A_0 = 0.08)$. The shaded region represents the wing-box area between the front and rear spars.

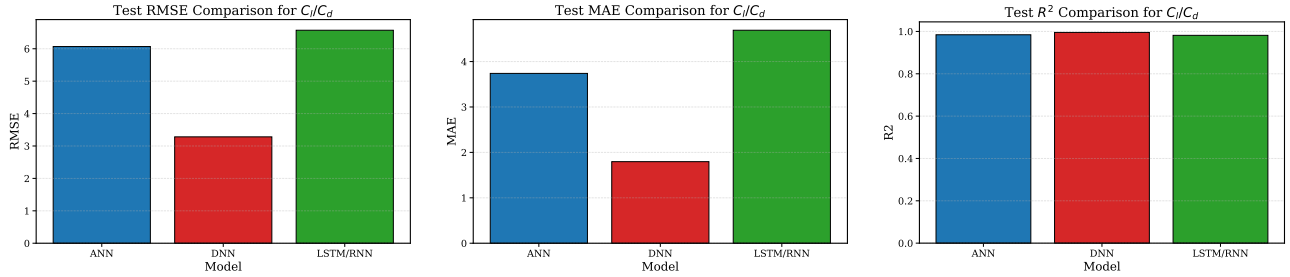
The constrained optimization results show that the CFD–Kriging framework can incorporate simplified aircraft-design requirements without causing a substantial loss in aerodynamic performance. The best feasible airfoil satisfies the prescribed wing-box constraint while retaining a lift-to-drag ratio close to the unconstrained optimum. This demonstrates that the proposed framework can support both maximum-performance searches and constrained aerodynamic optimization.

The CFD–Kriging results demonstrate the capability of the high-fidelity surrogate framework for verified forward optimization, inverse design, and constrained airfoil optimization at the selected design condition. The following subsection shifts the focus to the complementary XFOIL–ML framework.

4.6 Machine-Learning Model Performance

The predictive performance of the ANN, DNN, and LSTM/RNN models was evaluated using the independent airfoil-wise test dataset. Since the test set contains airfoil geometries that were not included during training or validation, the reported performance reflects the ability of each model to generalize to unseen airfoil shapes.

Figure 11 compares the test RMSE, MAE, and R^2 values for C_l/C_d prediction. Among the investigated architectures, the DNN achieved the best predictive accuracy, with the lowest RMSE and MAE and the highest coefficient of determination. Specifically, the DNN obtained RMSE = 3.281973 and $R^2 = 0.995417$, indicating excellent agreement with the XFOIL-generated reference data.



(a) RMSE. (b) MAE. (c) R^2.

Figure 11 – Comparison of ANN, DNN, and LSTM/RNN test performance for C_l/C_d prediction using RMSE, MAE, and R^2.

The ANN model provides good overall predictive capability, but its higher error indicates less accurate representation of the nonlinear C_l/C_d response compared with the DNN. The LSTM/RNN model also achieves good performance, but does not outperform the feedforward DNN. This suggests that, for the present input formulation and dataset size, increased nonlinear mapping capacity is more beneficial than explicit sequence modeling across the angle-of-attack sweep.

4.7 DNN-Based Forward Design and XFOIL Verification

Based on the model-performance comparison, the DNN was selected for the forward airfoil design study because it achieved the lowest prediction error and the highest R^2 value for C_l/C_d prediction. The objective was to identify the airfoil geometry and operating angle of attack that maximize the DNN-predicted lift-to-drag ratio within the prescribed XFOIL–ML design space.

The optimal design identified by the DNN and its independent XFOIL verification are summarized in Table 5. The predicted optimum corresponds to $m = 0.050000$, $p = 0.301214$, $t = 0.131875$, and $\alpha = 6.096841^\circ$, giving a maximum predicted value of $C_l/C_d = 192.322510$. Independent XFOIL re-evaluation at the same optimized angle of attack gives $C_l/C_d = 191.929556$, corresponding to a difference of only 0.20%.

Table 5 – DNN-based forward design optimum and XFOIL verification for maximum C_l/C_d.

m	p	t	α (deg)	C_l/C_d (DNN)	C_l/C_d (XFOIL)	**Difference (%)**
0.050000	0.301214	0.131875	6.096841	192.322510	191.929556	0.20

The geometry of the DNN-generated optimum is shown in Fig. 12. The optimized airfoil reaches the maximum allowable camber within the design space, with moderate thickness and an optimal operating angle of $\alpha = 6.0968^\circ$.

The close agreement between the DNN prediction and XFOIL re-evaluation confirms that the trained DNN can accurately guide the forward design search within the XFOIL-generated aerodynamic design space. However, this optimum should not be directly compared with the CFD–Kriging optimum because the CFD-based search was performed at a fixed angle of attack of $\alpha = 15^\circ$, whereas the DNN-based search optimizes both geometry and angle of attack using lower-fidelity XFOIL data.

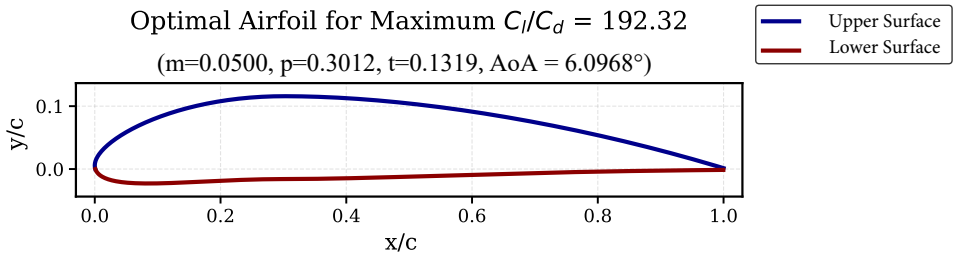


Figure 12 – DNN-generated optimal airfoil geometry corresponding to the maximum predicted $C_l/C_d = 192.32$.

4.8 Sensitivity Analysis

To interpret the trained DNN model, a permutation-based sensitivity analysis was performed to quantify the relative influence of each input variable on the predicted C_l/C_d. In this approach, each input feature is perturbed and the resulting change in predictive performance is evaluated. Larger importance values indicate stronger influence on the model output.

The resulting feature-importance values are shown in Fig. 13. The angle of attack is the dominant input, accounting for 57.024% of the total importance. This is expected because C_l/C_d varies strongly with operating condition over the wide angle-of-attack range considered in the XFOIL database. Among the geometric variables, maximum camber has the largest influence at 18.472%, followed by camber position at 13.769% and thickness ratio at 10.735%.

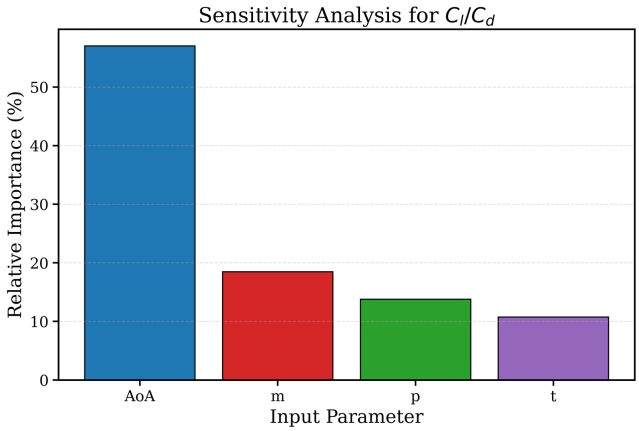


Figure 13 – Permutation-based feature importance of the DNN model for C_l/C_d prediction. The angle of attack is the dominant input, followed by maximum camber, camber position, and thickness ratio.

Overall, the sensitivity analysis confirms that the trained DNN captures both operating-condition effects and geometric effects. The following subsection compares the CFD–Kriging and XFOIL–ML frameworks and clarifies their complementary roles in the proposed design methodology.

4.9 Comparative Discussion of the CFD–Kriging and XFOIL–ML Frameworks

The two frameworks developed in this study serve complementary roles in aerodynamic airfoil design. The CFD–Kriging framework provides a high-fidelity surrogate-assisted approach based on validated CFD simulations, while the XFOIL–ML framework provides a larger data-driven environment for rapid aerodynamic prediction and preliminary design over a wider angle-of-attack range.

In the CFD-based framework, the Kriging surrogate was trained using 200 high-fidelity CFD samples at $\alpha = 15^\circ$ and $Re = 6 \times 10^6$. The surrogate achieved $R^2 = 0.9503$ and successfully supported forward optimization, inverse design, and wing-box-constrained optimization. The unconstrained optimum was verified by independent CFD with only 0.60% deviation, the inverse-design cases were verified with errors below 3%, and the constrained optimum retained a lift-to-drag ratio close to the unconstrained result.

In contrast, the XFOIL–ML framework was developed to evaluate data-driven aerodynamic prediction using a larger database of 10,200 samples over $-5^\circ \leq \alpha \leq 20^\circ$. Among the tested models, the DNN achieved the best predictive performance and accurately reproduced the XFOIL-verified optimum with a difference of approximately 0.20%. This demonstrates the usefulness of the XFOIL–ML framework for rapid model evaluation, sensitivity analysis, and preliminary design-space exploration.
The two optimum values should not be interpreted as directly comparable aerodynamic solutions because they are obtained under different modeling assumptions and operating conditions. The CFD–Kriging optimum is based on RANS CFD at a fixed angle of attack of $\alpha = 15^\circ$, whereas the XFOIL–ML optimum is obtained by optimizing both airfoil geometry and angle of attack using lower-fidelity XFOIL data. Therefore, the CFD–Kriging framework is most appropriate for CFD-verified optimization and constrained design at a selected operating condition, while the XFOIL–ML framework is most useful for rapid prediction and preliminary aerodynamic design.

5. Conclusions

This study developed an automated aerodynamic design framework for NACA four-digit airfoils by combining CFD-based surrogate optimization with XFOIL-based machine-learning prediction. The CFD setup was first validated using the NACA 0012 airfoil at $Re = 6 \times 10^6$, showing good agreement with experimental data and confirming the suitability of the numerical configuration for aerodynamic database generation.
A Python–ICEM–ANSYS Fluent workflow was implemented to generate a CFD database of 200 airfoil configurations at $\alpha = 15^\circ$. A Kriging surrogate model was trained to predict C_l/C_d as a function of the NACA design variables m, p, and t. The surrogate achieved $R^2 = 0.9503$ and supported forward optimization, inverse design, and wing-box-constrained optimization. The forward optimum was verified by independent CFD with a deviation of only 0.60%, the inverse-design targets were verified with errors below 3%, and the constrained optimum achieved only a 2.71% reduction relative to the unconstrained result.
A complementary XFOIL–ML framework was developed using 10,200 aerodynamic samples generated from 200 airfoils over 51 angles of attack. ANN, DNN, and LSTM/RNN models were trained and evaluated using an airfoil-wise train–validation–test split. The DNN achieved the best performance for C_l/C_d prediction, with RMSE = 3.281973 and $R^2 = 0.995417$. The DNN-based forward design was independently verified using XFOIL, giving a difference of approximately 0.20% between the predicted and re-evaluated optimum. Sensitivity analysis showed that angle of attack was the most influential input variable, followed by maximum camber, camber position, and thickness ratio.
The results demonstrate that the CFD–Kriging framework is effective for verified forward optimization, inverse design, and constrained aerodynamic optimization, while the XFOIL–ML framework provides rapid aerodynamic prediction and preliminary design capability over a broader operating range. The two frameworks should be interpreted as complementary rather than directly interchangeable because they use different aerodynamic fidelities and operating conditions.
The present study is limited to NACA four-digit airfoils, a fixed Reynolds number, and a fixed-angle CFD optimization condition. The wing-box constraint is also represented using a simplified two-dimensional internal-area proxy. Future work will extend the framework to variable Reynolds number and angle-of-attack conditions, broader airfoil parameterizations, three-dimensional wing configurations, and more detailed structural constraints.

6. Contact Author Email Address

The contact author email address is mailto: mohammad.alam.1@kfupm.edu.sa

7. Copyright Statement

The authors confirm that they, and/or their company or organization, hold copyright on all of the original material included in this paper. The authors also confirm that they have obtained permission, from the copyright holder of any third party material included in this paper, to publish it as part of their paper. The authors confirm that they give permission, or have obtained permission from the copyright holder of this paper, for the publication and distribution of this paper as part of the ICAS proceedings or as individual off-prints from the proceedings.

References

[1] D. Raymer. *Aircraft Design: A Conceptual Approach*. American Institute of Aeronautics and Astronautics, Inc., Reston, VA, 2012.

[2] Jan Roskam. *Airplane Design: Part 2-Preliminary Configuration Design and Integration of the Propulsion System*. DARcorporation, 1985.

[3] J. D. Anderson. *Aircraft Performance and Design*. WCB/McGraw-Hill, Boston, MA, 1999.

[4] Ira H Abbott and Albert E Von Doenhoff. *Theory of wing sections: including a summary of airfoil data*. Courier Corporation, 2012.

[5] Joaquim RRA Martins and Andrew Ning. *Engineering design optimization*. Cambridge University Press, 2021.

[6] Jerome Sacks, William J Welch, Toby J Mitchell, and Henry P Wynn. Design and analysis of computer experiments. *Statistical science*, 4(4):409–423, 1989.

[7] Donald R Jones, Matthias Schonlau, and William J Welch. Efficient global optimization of expensive black-box functions. *Journal of Global optimization*, 13(4):455–492, 1998.

[8] Alexander Forrester, Andras Sobester, and Andy Keane. *Engineering design via surrogate modelling: a practical guide*. John Wiley & Sons, 2008.

[9] K Sathyandra Rao, AN Abhilasha, Adrija Das, and M Sivapragasam. Aerodynamic shape optimization at low reynolds number using multi-level hierarchical kriging models. *Optimization and Engineering*, 26(1):479–505, 2025.

[10] Yu Zhang, Zhong-hua Han, and Wen-ping Song. An efficient robust aerodynamic design optimization method based on a multi-level hierarchical kriging model and multi-fidelity expected improvement. *Aerospace Science and Technology*, 152:109401, 2024.

[11] Brenda M Kulfan. Universal parametric geometry representation method. *Journal of aircraft*, 45(1):142–158, 2008.

[12] Dominic A Masters, Nigel J Taylor, TCS Rendall, Christian B Allen, and Daniel J Poole. Geometric comparison of aerofoil shape parameterization methods. *AIAA journal*, 55(5):1575–1589, 2017.

[13] MG Lauer and PJ Ansell. A review of parameterization methods for airfoil design. *Progress in Aerospace Sciences*, 158:101140, 2025.

[14] Xiaogang Liu, Shengyu Yang, Haifeng Sun, Zhongyi Wang, Xue Guan, Yuanqi Gu, and Yuhang Wang. Review of deep learning-based aerodynamic shape surrogate models and optimization for airfoils and blade profiles. *Physics of Fluids*, 37(4), 2025.

[15] Peter Sharpe and R John Hansman. Neuralfoil: An airfoil aerodynamics analysis tool using physics-informed machine learning. *arXiv preprint arXiv:2503.16323*, 2025.

[16] Chinmayi Siddamsetty, D Jyothika, Tabindah Saleem, P Manvitha, HV Srikanth, and S Vijay Kumar. Prediction of airfoil efficiency by artificial neural network. In *International Conference on Emerging Research in Computing, Information, Communication and Applications*, pages 1–14. Springer, 2023.

[17] Diana-Andreea Sterpu, Daniel Măriuța, Grigore Cican, Ciprian-Marius Larco, and Lucian-Teodor Grigorie. Machine learning prediction of airfoil aerodynamic performance using neural network ensembles. *Applied Sciences*, 15(14):7720, 2025.

[18] Chao Chen, Bohan Zhang, Hongyu Huang, Zhijiang Xie, Chuan Yang, Dehong Meng, Hao Yue, and Lei Liang. A multi-task learning framework for aerodynamic computation of two-dimensional airfoils. *Physics of Fluids*, 36(11), 2024.

[19] Xin Hu, Bo An, Yongke Guan, Dong Li, Fernando Mellibovsky, Weimin Sang, and Gang Wang. Enhancing airfoil design optimization surrogate models using multi-task learning: Separating airfoil surface and fluid domain predictions. *Physics of Fluids*, 37(3), 2025.

[20] Yubiao Sun, Ushnish Sengupta, and Matthew Juniper. Physics-informed deep learning for simultaneous surrogate modeling and pde-constrained optimization of an airfoil geometry. *Computer Methods in Applied Mechanics and Engineering*, 411:116042, 2023.

[21] Bo Li, Shuyu Lin, Jun Yang, Shuo Chen, Damin Cao, and Jiayi Zhao. Inverse design model of airfoil based on long short-term memory neural network by fusing multi-position data. *Physics of Fluids*, 37(10), 2025.

[22] JMJ Fray, JW Slooff, JW Boerstoel, and A Kassies. Inverse method with geometric constraints for transonic aerofoil design. *International journal for numerical methods in engineering*, 22(2):327–339, 1986.

[23] Mark Drela. Xfoil: An analysis and design system for low reynolds number airfoils. In *Low Reynolds number aerodynamics: proceedings of the conference notre dame, Indiana, USA, 5–7 June 1989*, pages 1–12. Springer, 1989.

[24] Charles L. Ladson. Effects of independent variation of mach and reynolds numbers on the low-speed aerodynamic characteristics of the NACA 0012 airfoil section. NASA Technical Memorandum 4074, National Aeronautics and Space Administration, Langley Research Center, Hampton, Virginia, 1988. Accession ID: 19880019495.

[25] C. L. Ladson, C. W. Brooks, A. S. Hill, and D. W. Sproles. Computer program to obtain ordinates for NACA airfoils. Technical Report Technical Report 4741, NASA, 1996.

[26] M. D. Morris and T. J. Mitchell. Exploratory designs for computational experiments. *Journal of Statistical Planning and Inference*, 43(3):381–402, 1995.